THE SIMULATION OF THE DEFORMATION AND BREAKING OF OCEAN WAVES IN WAVE GROUPS

M. P. TULIN, Y. YAO and P. WANG

Ocean Engineering Laboratory
University of California, Santa Barbara, CA 93117

ABSTRACT

Energetic long crested ocean waves are simulated through exact inviscid numerical calculations, using techniques especially designed for that purpose; trains of $O(10^2)$ waves can be accurately simulated; surface tension is neglected. The resulting numerical wave tank, LONGTANK, has been used to study the evolution of wave groups, the deformation of waves in passing through the peak of the wave groups, the inception of breaking, jet formation at the crest of breaking waves, the evolution of the jet into a breaker,and its reentry into the surface ahead of the crest, creating vorticity. Breakers are followed throughout their history. The wave momentum and energy lost in the breakers is estimated as well as the vorticity generated. The wave crest is shown to be amplified for the breaking wave. The ratio of maximum crest height to significant wave height is estimated to depend upon the wave age, with a maximum value around 1.6 for developing seas.

KEYWORDS

Numerical wave tank, wave grouping, wave deformation, breaking, breaker, breaker vorticity, breaking dissipation, maximum crest height,

INTRODUCTION

The development of numerical means to investigate unsteady non-linear gravity waves has received considerable attention since the pioneering work of Longuet-Higgins and Cokelet (1976), who used the Boundary Integral (or Element) Method, BEM, together with a mixed Eulerian-Largrangian technique, MEL, to simulate the initial overturning of periodic steep gravity waves subject to an impressed pressure on the free surface behind the crest. Their method has been adopted for the study of non-linear interaction and breaking of wave trains containing a limited number of waves (order of 10) arranged periodically (Dold and Peregrine, 1986b); a considerable effort has been made to improve numerical stability and computational efficiency (Vinje and Brevig, 1981; Dold and Peregrine, 1986a). The former authors have also simulated the rolling motion of a floating body in non-linear propagating waves.

The numerical simulation of nonlinear waves created in a tank by a wavemaker has first been carried out by Lin *et al* (1984), and subsequently by Dommermuth *et al* (1987), Grilli *et al* (1989), and by Cointe (1990), again for a small number of waves, O(10), with either a numerical beach or linear radiation open boundary conditions.

It is an inherent property of the BEM that a full matrix of influence coefficients must be used, and, as a result, the computing time per time step increases quadratically with the number of nodes on the free surface; this fact has previously prevented the high resolution computation of $O(10^2)$ waves, although

this is an essential requirement for a numerical wave tank capable of the detailed study of non-linear wave interaction phenomena.

We have developed a two-dimensional numerical wave tank, Figure 1, called LONGTANK; a tank length of 110 wave lengths has been achieved, utilizing a multi-subdomain, MSD, modification of the BEM (Wang *et al*, 1993). The optimized MSD approach (Wang, 1993) features matrix block-diagonalization, which reduces the number of influence coefficients by two orders of magnitude in the cases we typically deal with, achieves high computational efficiency and leads to a computing time per time step increasing linearly with increase in the number of free surface nodes.

LONGTANK has been used to calculate the progress of unstable gravity wave systems toward deformation and breaking both in deep and shallow water. Strongly modulated wave groups and wave breaking near the group peak have been observed as well as breaking at the front of the group. A consistent inception condition for wave breaking in the wave groups has been found through these simulations.

The high resolution and accuracy achieved in the simulation permits continuation of computation up to and beyond the point where the breaking jet touches the free surface. The local analysis of the particle motion reveals that particles near the tip of the jet almost exactly follow a ballistic trajectory, which tends to confirm the accuracy of simulation.

The newly developed numerical technique, taking advantage of the multi-subdomain approach, allows the continuation of the calculation beyond the initial splash. Preliminary results show the touchdown of the jet on the free surface beyond the crest, and as a result, the generation of circulation in around the enclosed-bubble, as well as at the jet-free surface contact line. The simulation allows the quantification of the vorticity created in this way during breaking. We have estimated that this vorticity will have a significant effect on the immediately following waves.

The energy and momentum lost to the wave motion due to the breaker has also been quantified. Further study of these losses could give a better understanding of breaking dissipation and of the frequency downshifting mechanism, both very important in ocean wave modelling.

Due to strong group modulation, wave energy concentrates near the peak of the group. The simulation shows that strong deformation of the waveform occurs at the group peak, just before breaking. Both the wave trough and crest rise significantly. The simulations reveal a larger wave asymmetry than commonly used in engineering applications. A simple model has been proposed to predict maximum wave and crest height, which gives maximum values in the range which has been observed for so called "freak" waves in the ocean (Sand *et al*, 1990).

WAVE GROUP FORMATION

Finite amplitude wave trains are subject to Benjamin-Feir instability, leading to the growth of side bands and strong group formation. An example is shown in Figure 2, where a plunging wavemaker creates a wave system consisting initially of a carrier wave of steepness (ak), 0.14, together with the two most rapidly growing sidebands; the initial energy in each of the sidebands is 1% of the the energy in the carrier wave. Downtank, increasingly strong wave group formation occurs, with groups of about 3.5 waves. The peaks of the wave group travel with the group velocity, $c_g \approx c_p/2$, while each individual wave travels with the phase speed, c_p.

BREAKING AND THE INCEPTION CONDITION

An example of LONGTANK simulation with strong wave grouping leading to wave deformation and breaking, is shown in Figure 3. The initial wave steepness in this case is 0.19. With continual suppression of possible breaking at the front of the wave train using the 'peeling' technique (Wang *et al*, 1993), wave breaking eventually occurs in the center of the second group after 58 wave periods. The wave deformation in the initial stage of breaking is shown in Figure 4. A strong fore and aft wave

form asymmetry is found at breaking, with an elevation of the forward trough . The time to breaking in this stage and the shape of the waves compare very well with the photographs of Bonmarin et al (1985), see Figure 11 of Wang *et al* 1993.

The horizontal particle velocity at the crest changes slowly as the wave progresses through the group, but when and only when this particle speed reaches a value of the group velocity (inception), a very rapid increase in this speed occurs accompanied by a strong wave deformation; then a small jet forms at the crest, its speed reaches a value of about $1.1c_p$, and it forms a small spilling breaker. The interval between inception and breaking is less than half the wave period.

The same general phenomena appears in all simulations where breaking occurs within the wave train, in both deep and shallow water. In particular, the inception of the breaking invariably corresponds to the condition that the particle speed at the wave crest reaches the group speed, see Figure 5.

WAVE DEFORMATION AND FRONT FACE STEEPENING

The wave deformation following breaking inception (crest particle speed equals c_g) closely resembles the pre-breaking deformations observed at sea by Kjeldsen and Myrhaug (1980) : wave shortening and steepening before the crest, trough rising. These authors devised a deformation parameter, $[\eta'/H][\lambda/\lambda']$, see Figure 6, and suggested, based on tank tests, that values larger than 3.5 correspond to breaking conditions. We have found values in the range 3.48 - 5.29 just prior to breaking (see table 8.2 of Wang, 1993).

BREAKER MORPHOLOGY

In Figure 7 is shown an example of wave breaking occurring inside the wave group near the group peak. The time from steepening of the front face to the initiation of the splash is only about a tenth of the wave period, in this case. With the formation of a jet and its successive free fall, the crest height decreases.

The initial stage of jet closure and splash is shown in Figure 8, for another case. The tangential velocity along the boundary of the new closed bubble and at the common interface near the tip of the jet has been indicated; the circulation, Γ, has been calculated to yield a value of $0.038\lambda c_p$ (clock wise). To evaluate the influence of this generated vorticity on the following waves, we assume that the vorticity (Ω) corresponding to Γ, is uniformly distributed in the area S, under the wave crest and lying above the mean water level ($S = a\lambda/\pi$). Therefore $\Omega = \Gamma/S \approx 0.12\ c_p/a \approx [0.12/(ak)]\ \omega$, where ω is the wave frequency and k is the wave number. For linear deep water waves, with amplitude a and wave frequency ω, the strain rate, $\partial u/\partial x$, at the wave crest is $(ak)\omega$. Therefore for a wave with a steepness $(ak) \approx 0.2$, the strain rate due to the breaker vorticity, Ω, is three times larger than that from the potential wave itself. As rough as this calculation is, it indicates the probable importance of the breaker vorticity in effecting the behavior of the following waves.

The calculation of the motion much beyond splash is difficult, even without invoking the breakdown of the flow there to turbulence. However, it is possible to continue the calculation as if the jet does not see the free surface, see Figure 9; this is the same case as shown in Figure 10. In this way we can learn that breaking can in principle continue well beyond the initiation of the splash. In fact, Figure 9 corresponds roughly to the condition that the initial splash has been overrun by the wave crest and is being ingested.

The breaking jet also removes momentum from the wave and this must find its way into the drift current beneath the wave. Up to the stages calculated in Figures 8 and 9, the small jet already contains about one to two tenths of both the wave energy and momentum in a single wavelength, showing the significance of breaking as a source of conversion of wave energy into turbulence and surface drift.

The local particle motion has also been studied in the simulations, showing that the particles near the tip of the jet almost exactly follow ballistic trajectories, see Figure 10. This should certainly be expected

since the pressure throughout the falling jet must be very close to atmospheric, leaving gravity as the dominant influence on the particle motion. The calculated ballistic trajectories thus tend to confirm the accuracy of the numerical calculation throughout the breaking stage.

We would also like to share with readers one special case we have experienced, where the behavior of the breaking jet seems anomalous, Figure 11; as can be seen, beneath the initial jet, another jet forms.

EXTREME WAVE CREST HEIGHT

Strong wave grouping concentrates the energy in the center of the wave group, increasing the wave height, which is then further enhanced by the wave deformation which accompanies breaking. The tank experiment of Su & Green (1985) provides measurements of the maximum wave steepness ($h_m k/2$) at breaking in wave groups, for various values of initial wave steepness; these results are also presented in our previous paper (Wang *et al*, 1993) together with similar results from LONGTANK simulations.

In our simulations, for a strongly deformed wave, the horizontal asymmetry factor, μ, (the ratio between the crest and wave height) is found to have an average value of 0.79, larger than the value of 0.6 normally suggested for engineering application (Stansberg, 1991). Kjeldsen (1990) suggested, based on their tank experiments, that the inception of breaking occurred for $\mu > 0.77$.

With this knowledge, we can construct a simple model to predict extreme wave and crest heights. Assuming a wave train with an average wave height equal to the significant wave height in a given sea state, strong modulation and breaking deformation will lead to the greatest wave and crest heights at the group peaks. The significant wave steepness as a function of wave age can be deduced from Toba's 3/2-power law (Toba, 1972), which is, $(ak)_s^2 \approx 2\pi^3 B \left(\frac{u_*}{c_s}\right)$, where u_* is the friction velocity and c is the wave speed, subscript s denotes the significant wave, and B is Toba's constant (0.062).

Combining this formula with Su's results and the asymmetry factor, 0.79, the ratios of maximum wave height and crest height to significant wave height versus wave age can be obtained, see Figure 12, where a mean and an extreme prediction have been indicated, depending on statistical uncertainties in both experiments and simulations. It is seen that for developed ocean waves, the maximum wave crest height lies in the range around 1.6 times the significant wave height. Ratios of wave crest height to significant wave height of this magnitude have been observed in the ocean (Sand *et al*, 1990, and A. K. Magnusson, DNMI, private communication). It is clear that prediction of the maximum wave crest height is very important for the specification of offshore structures, and we intend to pursue this matter further.

ACKNOWLEDGEMENT

The authors are grateful for support from the Office of Naval Research, Ocean Technology Program, directed by Dr. Thomas Swean.

REFERENCES

Bonmarin, P. and Ramamonjiarisoa, A. (1985). Deformation to breaking of deep water gravity waves. *Experiments in Fluids*, 3, 11-16

Cointe, R. (1990). Numerical simulation of a wave channel. *Engineering Analysis with Boundary Elements*, 7, 167-177

Dold, J.W. and Peregrine, D.H. (1986a). An efficient boundary-integral method for steep unsteady water waves. *Numerical Methods for Fluid Dynamics II* (K.W. Morton and M.J. Baines Ed.), 671-679

Dold, J.W. and Peregrine, D.H. (1986b). Water-wave modulation. *Proc. 20th Int. Conf. on Coastal Eng.* (Taipeh), I, 163-175

Dommermuth, D.G., Yue, D.P., Lin. W.M., Rapp, R.J., Chan, E.S. and Melville, W.K. (1988). Deep-water plunging breakers: a comparison between potential theory and experiments. *J. Fluid Mech.*, 189, 423-442

Grilli, S.T., Skourup, J. and Svendsen, I.A. (1989). An efficient boundary element method for nonlinear water waves. *Engineering Analysis with Boundary Elements*, 6 no. 2, 97-107

Kjeldsen, S.P. and Myrhaug, D. (1980). Wave-wave interactions, current-wave interaction and resulting extreme waves and breaking waves. *Proc. 17th Coastal Eng. Conf.* 2277-2303

Kjeldsen, S.P. (1990). Breaking waves. *Water Wave Kinematics* (A. Torum and O.T. Gudmestad Ed.), 453-473

Lin, W.M., Newman, J.N. and Yue, D.K.P. (1984). Nonlinear forced motions of floating bodies. *Proc. 15th Symp. on Naval Hydro.* (Hamburg), 33-49

Longuet-Higgins, M.S. and Cokelet, E.D. (1976). The deformation of steep surface waves on water. I. A numerical method of computation. *Royal Soc. London A*, 350, 1-26

Sand, S.E., Hansen, N.E.O., Klinting, P., Gudmestad, O.T. and Sterndorff M.J. (1990). Freak wave kinematics. *Water Wave Kinematics* (A. Torum and O.T. Gudmestad Ed.), 535 -549

Stansberg, C.T. (1991). Extreme wave asymmetry in full scale and model scale experimental wave trains. *Proc. OMAE*, 1-A, 215-222

Su, M.Y. and Green, A.W. (1985). Wave breaking and nonlinear instability coupling. *The Ocean Surface* (Y. Toba and H. Mitsuyas Ed.), 31-38

Vinje, T. and Brevig, P. (1981). Numerical simulation of breaking waves. *Adv. Water Resources*, 4, 77-82

Wang, P., Yao, Y. and Tulin, M.P. (1993). Wave group evolution, wave deformation, and breaking: simulation using LONGTANK, a numerical wave tank. *Proc. Third Int. Offshore and Polar Engr. Conf.* III, 27-33. *J. Offshore and Polar Engr.* (In press).

Wang, P. (1993). Numerical research on (I) Ship internal waves, and (II) Breaking waves. *Ph.D Dissertation*, (Univ. of California, Santa Barbara).

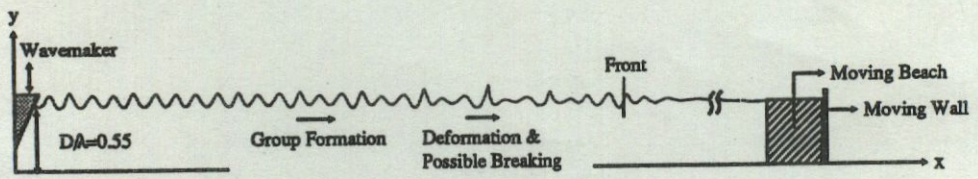

Fig. 1 : Schematic of the nonlinear numerical wave tank — *LONGTANK*

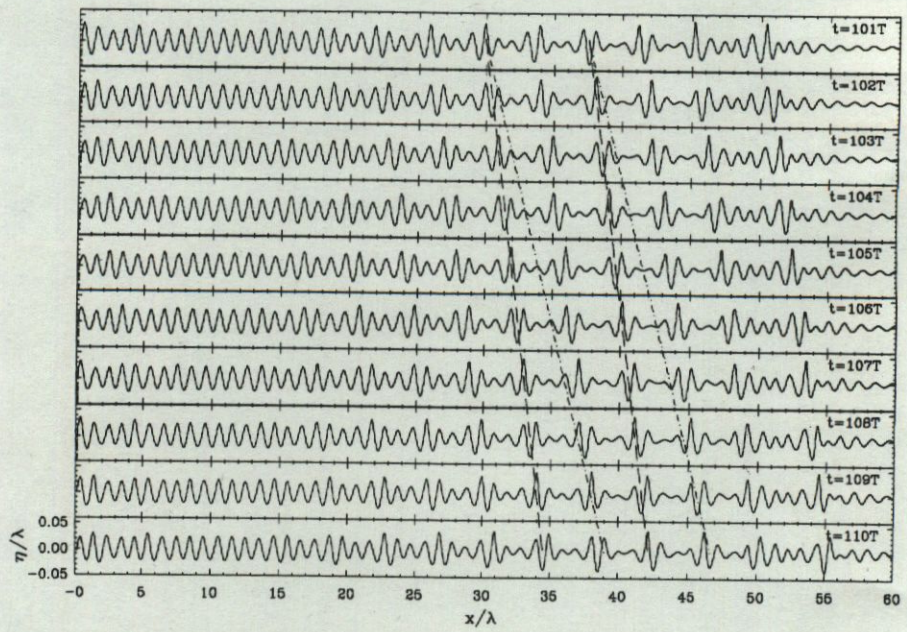

Fig. 2 : Simulated wave train (left to right), $(ak)_o = 0.14$. Dashed lines indicate propagation at the group velocity (- - -) and phase velocity (- · -).

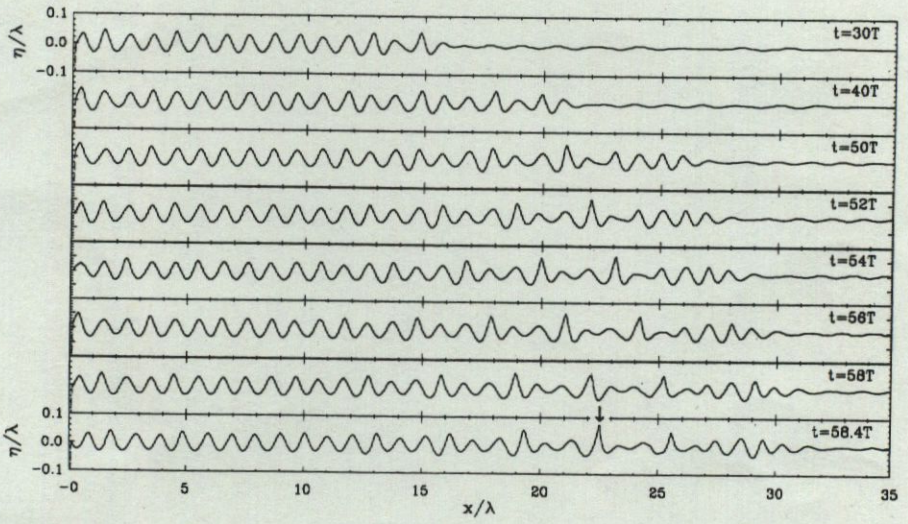

Fig. 3 : Side-band modulation leads to wave grouping, wave deformation and eventually breaking in the area denoted by ↓. The breaking area is blown up in Fig. 4. $(ak)_o = 0.19$

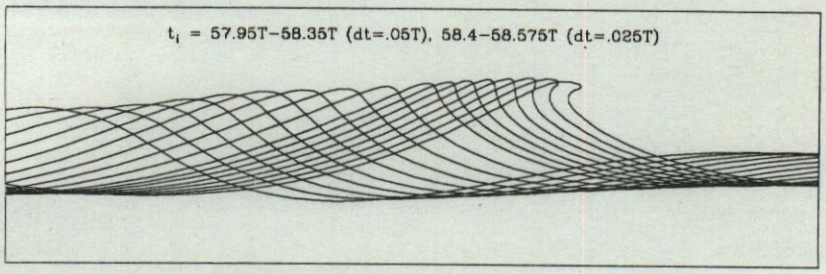

Fig. 4 : Wave deformation and breaking, $(ak)_o = 0.19$: strong fore and aft asymmetries

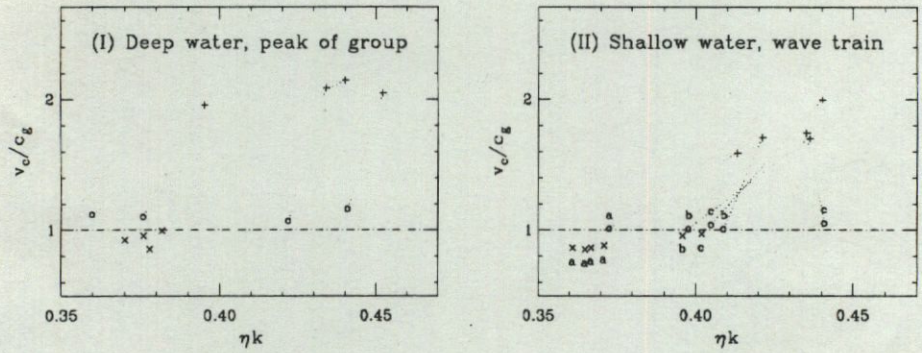

Fig. 5 : Particle velocity at crest (v_c/c_g) vs. wave steepness (ηk). Showing a criterion of wave breaking within group (I) or wave train in (II). Symbols: (- · -), threshold line indicating inception of breaking; (x), achieving local maximum and decreasing; (o), tending to breaking inevitably; (+), breaking. In (II) : a, kD = 1, $c_g/c_p = 0.77$; b, kD = 1.2, $c_g/c_p = 0.74$; c, kD = 1.4, $c_g/c_p = 0.7$

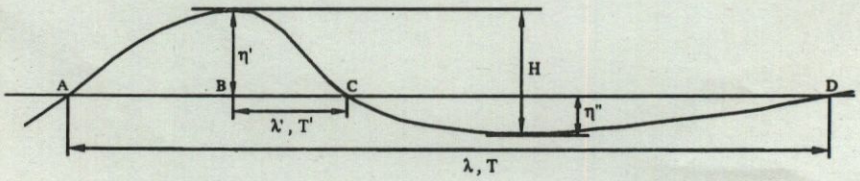

Fig. 6 : Geometry of wave profile

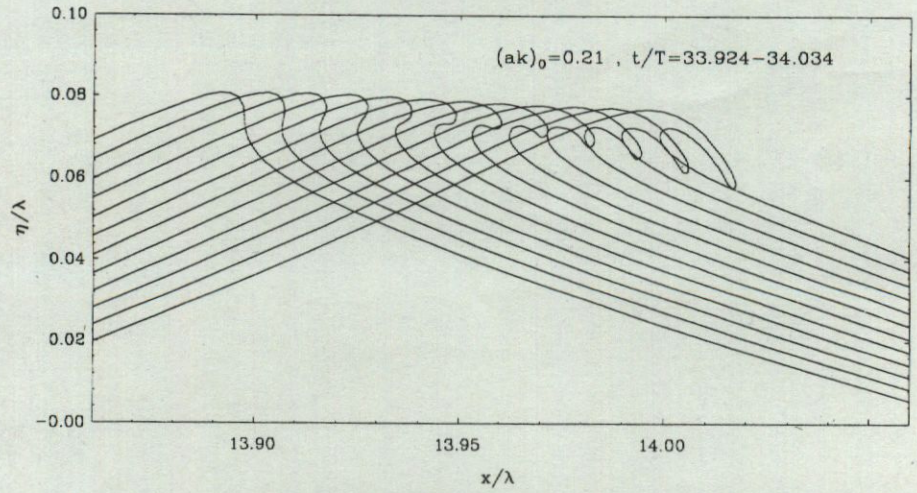

Fig. 7 : Wave breaking in *LONGTANK*, showing the formation of a plunging jet

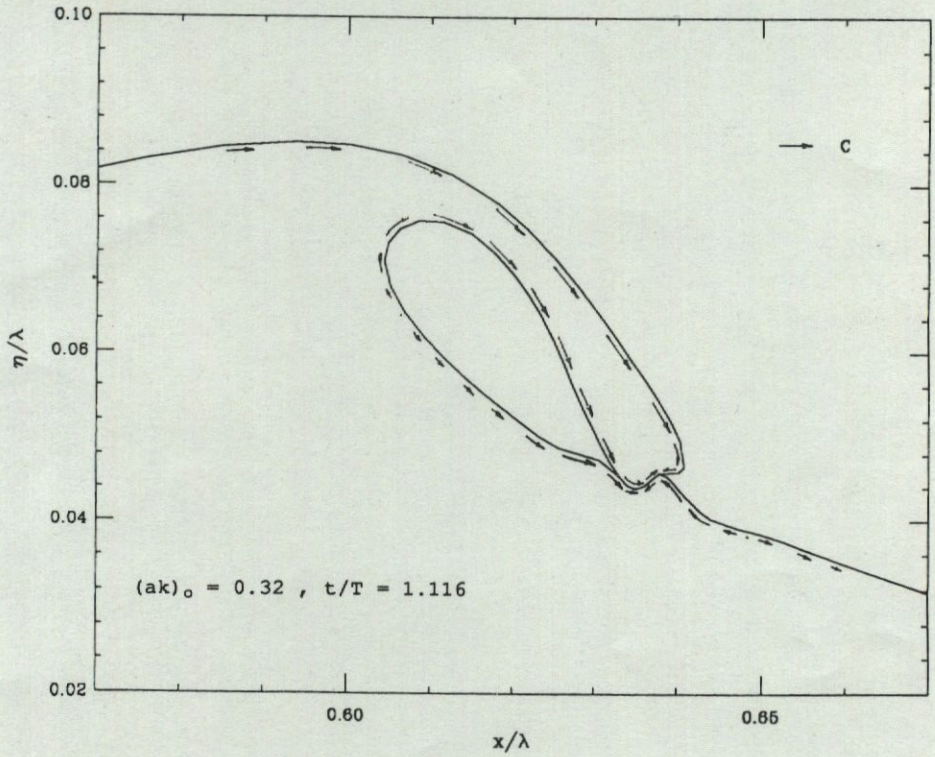

Fig. 8 : Initial stage of jet closure and splash. The tangential velocity around the jet is indicated

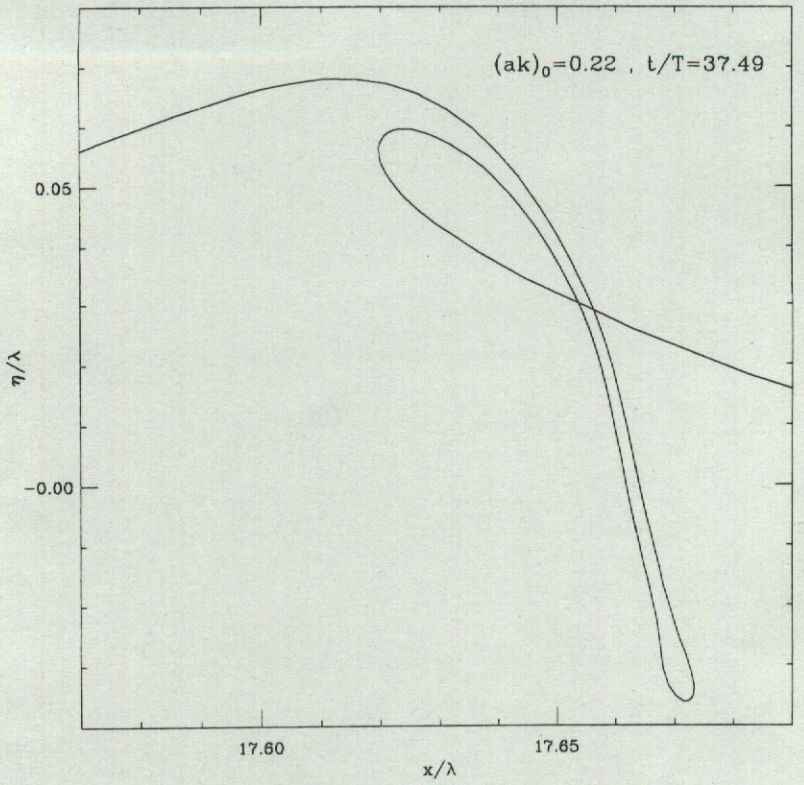

Fig. 9 : Jet free fall as if it does not see the free surface

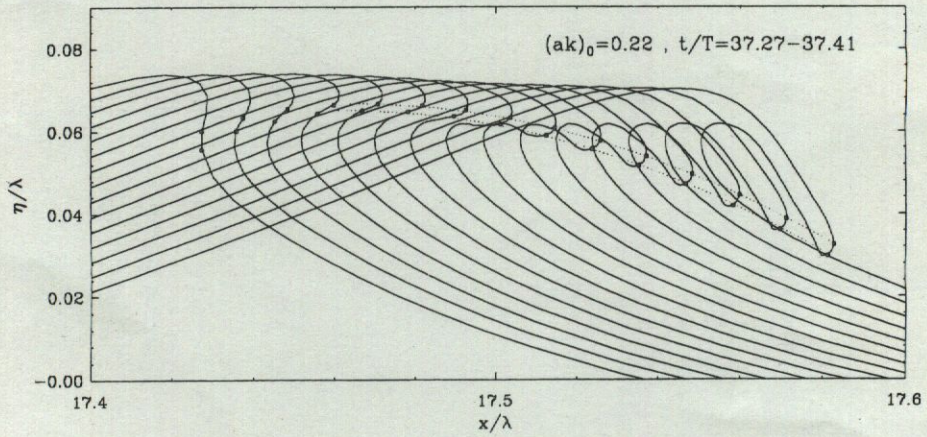

Fig. 10 : Evolution of a plunging jet, preceding figure 9. ····· ballistic particle trajectories (estimated); the large dots (•) indicate the actual particle position.

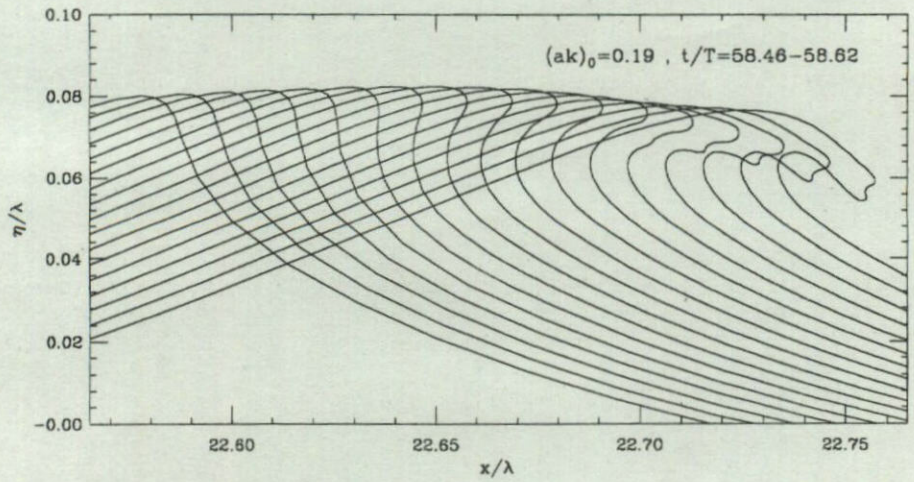

Fig. 11 : Anomalous double jet

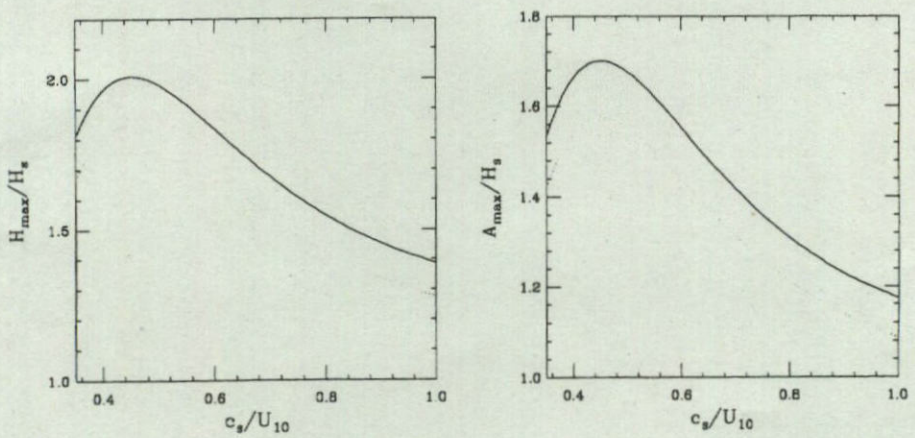

Fig. 12 : Predicted maximum wave height, H_{max}, and crest elevation, A_{max}, as a function of wave age, c_s/U_{10}. H_s, significant wave height; c_s, wave speed at spectral peak; U_{10}, wind speed at 10m. —— extreme prediction; ····· medium prediction.

AN EXPERIMENTAL STUDY OF NON-LINEAR WAVE-CURRENT INTERACTIONS

I. CUMMINS and C. SWAN

Department of Civil Engineering , Imperial College, London,
SW7 2BU, United Kingdom.

ABSTRACT

This paper presents the results of a new laboratory investigation in which a series of progressive gravity waves were superimposed upon a strongly sheared co-flowing current. The direction of this current was reversible allowing the formation of a "favourable" current (in the same direction as the phase velocity), or an "adverse" current (in the opposite direction to the phase velocity). The experimental data shows that both the wave kinematics and pressure fluctuations are strongly dependent upon the non-linear wave-current interaction. If design calculations are based upon either an irrotational wave solution or an irrotational wave-current solution, both the underlying kinematics and pressure fluctuations will be incorrectly predicted. However, the present data suggests that a fully non-linear wave-current solution, similar to that proposed by Dalrymple and Heideman (1989), Chaplin (1990) and Cummins and Swan (1993) will provide a good description of the entire flow field.

INTRODUCTION

Wave-current interactions are an important feature of most marine environments and have been the subject of a sustained research effort. When a wave train first propagates onto a current there is a transfer of energy between the wave and the current. This corresponds to the so called "transient" (or unsteady) stage in which there is a change in the energy density of the wave train, and a corresponding adjustment in the wave height. Beyond this region an "equilibrium" condition is established in which the wave co-exists with the current. It is this latter stage which the present investigation will consider.

It is well known that the equilibrium state associated with the interaction of waves and currents is dependent upon the variations in the current profile with depth, $U(z)$. For example, in many tidal flows the current profile is approximately uniform with depth, $U(z)$=constant. In these cases the wave remains irrotational, and the combined flow field is simply given by the linear sum of the current velocity and the wave induced kinematics. In effect, the only interaction occurs within the associated dispersion equation and a "Doppler shifted solution" results. This case has been considered by Fenton (1985) in which he presented an "alternative Stokes theory" valid to a fifth order of wave steepness. The interaction of waves on a linear shear current, (dU/dz=constant) has also been considered by a number of authors including Dalrymple (1974) and Kishida and Sobey (1988). In this case the time-averaged vorticity is constant throughout the flow field, and calculations